



Article

Sesamol Ameliorates Renal Injury-Mediated Atherosclerosis via Inhibition of Oxidative Stress/IKK α /p53

Jie-Sian Wang^{1,2,†}, Ping-Hsuan Tsai^{1,†}, Kuo-Feng Tseng³, Fang-Yu Chen¹, Wen-Chin Yang⁴
and Ming-Yi Shen^{1,5,6,*}

- ¹ Graduate Institute of Biomedical Sciences, China Medical University, Taichung 40402, Taiwan; d29745@mail.cmuh.org.tw (J.-S.W.); u105010312@cmu.edu.tw (P.-H.T.); fyc0321@gmail.com (F.-Y.C.)
² Division of Nephrology, Department of Internal Medicine, China Medical University Hospital, Taichung 40402, Taiwan
³ Department of Biological Science and Technology, China Medical University, Taichung 40402, Taiwan; u107010409@cmu.edu.tw
⁴ Agricultural Biotechnology Research Center, Academia Sinica, 128, Sec. 2, Academia Rd., Nankang, Taipei 115, Taiwan; wcyang@gate.sinica.edu.tw
⁵ Department of Medical Research, China Medical University Hospital, Taichung 40402, Taiwan
⁶ Department of Nursing, Asia University, Taichung 41354, Taiwan
* Correspondence: shenmy@mail.cmu.edu.tw or shenmy1124@gmail.com; Tel.: +886-4-2205-3366 (ext. 5809)
† These authors equally contributed to this study.



Citation: Wang, J.-S.; Tsai, P.-H.; Tseng, K.-F.; Chen, F.-Y.; Yang, W.-C.; Shen, M.-Y. Sesamol Ameliorates Renal Injury-Mediated Atherosclerosis via Inhibition of Oxidative Stress/IKK α /p53. *Antioxidants* **2021**, *10*, 1519. <https://doi.org/10.3390/antiox10101519>

Academic Editors: Natalia Di Pietro and Mario Bonomini

Received: 6 August 2021

Accepted: 22 September 2021

Published: 24 September 2021

Publisher's Note: MDPI stays neutral with regard to jurisdictional claims in published maps and institutional affiliations.



Copyright: © 2021 by the authors. Licensee MDPI, Basel, Switzerland. This article is an open access article distributed under the terms and conditions of the Creative Commons Attribution (CC BY) license (<https://creativecommons.org/licenses/by/4.0/>).

Abstract: Patients with chronic kidney disease (CKD) are at an increased risk of premature death due to the development of cardiovascular disease (CVD) owing to atherosclerosis-mediated cardiovascular events. However, the mechanisms linking CKD and CVD are clear, and the current treatments for high-risk groups are limited. In this study, we aimed to examine the effects of sesamol, a natural compound extracted from sesame oil, on the development of atherosclerosis in a rodent CKD model, and reactive oxygen species-induced oxidative damage in an endothelial cell model. ApoE^{-/-} mice were subjected to 5/6 nephrectomy (5/6 Nx) and administered sesamol for 8 weeks. Compared with the sham group, the 5/6 Nx ApoE^{-/-} mice showed a significant increase in malondialdehyde levels and Oil Red O staining patterns, which significantly decreased following sesamol administration. Sesamol suppressed H₂O₂-induced expression of phospho-IKK α , p53, and caspase-3. Our results highlight the protective role of sesamol in renal injury-associated atherosclerosis and the pathological importance of oxidative stress burden in CKD–CVD interaction.

Keywords: atherosclerosis; apoptosis; chronic kidney disease; sesamol; reactive oxygen species

1. Introduction

Patients with chronic renal failure are at an increased risk of premature mortality, which is associated with an increased incidence of atherosclerotic cardiovascular complications [1]. Atherosclerosis and cardiovascular diseases (CVDs) occur due to the imbalances between the production and scavenging of free radicals during physiological processes, thereby leading to inflammation, apoptosis, and lipid, protein, or nucleic acid damage [2]. Oxidative stress is caused by excessive reactive oxygen species (ROS), including hydroxyl radicals and superoxide anions [2]. Chronic kidney disease (CKD) is associated with high levels of ROS generation [3]. ROS might contribute to renal injury progression and atherosclerosis pathogenesis in CKD. Hydrogen peroxide (H₂O₂) is a major ROS generated during ischemia–reperfusion injury and is produced in animal models of chronic brain disease [4]. H₂O₂ can induce oxidative stress in endothelial cells, causing cell dysfunction and apoptosis [5,6]. Endothelial cells have a fundamental role in various pathological and physiological processes. For instance, they can synthesize and release catecholamines in response to ischemia, highlighting their importance in controlling vascular homeostasis [7]. Therefore, interventions that inhibit

ROS-induced endothelial cell damage can benefit patients with CKD and CVD [3,8]. Oxidative stress can be alleviated by antioxidant therapies using vitamin C, vitamin E, and other natural antioxidants.

There is a growing interest in the development of effective cardiovascular therapeutic drugs, especially those of natural origin, owing to their lack of adverse effects and effects on a variety of disease targets [9,10]. Sesamol (SM), a predominant active component of sesame seed oil, has been recognized as a health food, and has been used as a traditional medicine for several years [11]. It is a safe, non-toxic, organic compound that mediates anti-inflammatory effects via the downregulation of inflammatory marker transcription, such as cytokines, protein kinases, enzymes that promote inflammation, and redox status [12,13]. Sesamol also possesses other therapeutic properties, including anti-cancer [14], anti-aging [15], anti-atherosclerotic [11], hepatoprotective [16], and anti-acute renal injury [17] effects. Although recent studies have demonstrated that SM supplementation acts as a potent adjuvant to treat acute renal injury owing to its prophylactic protective effects [17] and vascular protective effects [18–20], the mechanisms by which SM protects against renal injury-associated atherosclerosis and protects endothelial cells from oxidative stress injury remain unclear. In this study, we aimed to explore the mechanisms by which SM exerts its therapeutic effects on atherosclerosis in a chronic renal failure model and its effect on endothelial functions to identify alternative therapeutic interventions for cardiovascular complications in patients with CKD.

2. Materials and Methods

2.1. Reagents, Antibodies, and Cells

SM (5-hydroxy-1,3-benzodioxole; purity: 99.9% by GC) (Figure 1A), dimethylsulfoxide (DMSO), H₂O₂, and 3-(4,5-di-methylthiazol-2-yl)2,5-diphenyltetrazolium bromide (MTT) were procured from Sigma (St. Louis, MO, USA). IKK α siRNA (si-IKK α) and control siRNA (si-Ctl) were bought from Santa Cruz Biotechnology (Santa Cruz, CA, USA). Human aortic endothelial cell line (HAEC), derived from a human heart aorta, was obtained from Promo Cell (Heidelberg, Germany).

2.2. Animal Model and Experimental Design

All mice experiments were approved by the China Medical University Institutional Animal Care and Use Committee, and were conducted in accordance with the Guide for the Care and Use of Laboratory Animals of the US National Institutes of Health (NIH Publication No. 85–23, revised 1996). Subtotal 5/6 nephrectomy (5/6 Nx) was performed on 10–12-week-old female ApoE^{-/-} mice under isoflurane inhalation anesthesia with total removal of the right kidney and selective infarction of approximately 2/3 of the left kidney by ligating two or three renal artery branches. Female ApoE^{-/-} mice were utilized because of an increased incidence of atherosclerosis in females compared to males [21]. The mice were fed a regular chow diet throughout the study. The mice received SM (25 and 50 mg/kg, SM25 and SM50, respectively) by oral gavage three times per week for 8 weeks after 5/6 Nx surgery. All mice were sacrificed via isoflurane inhalation followed by cervical dislocation [21] (Figure 1B).

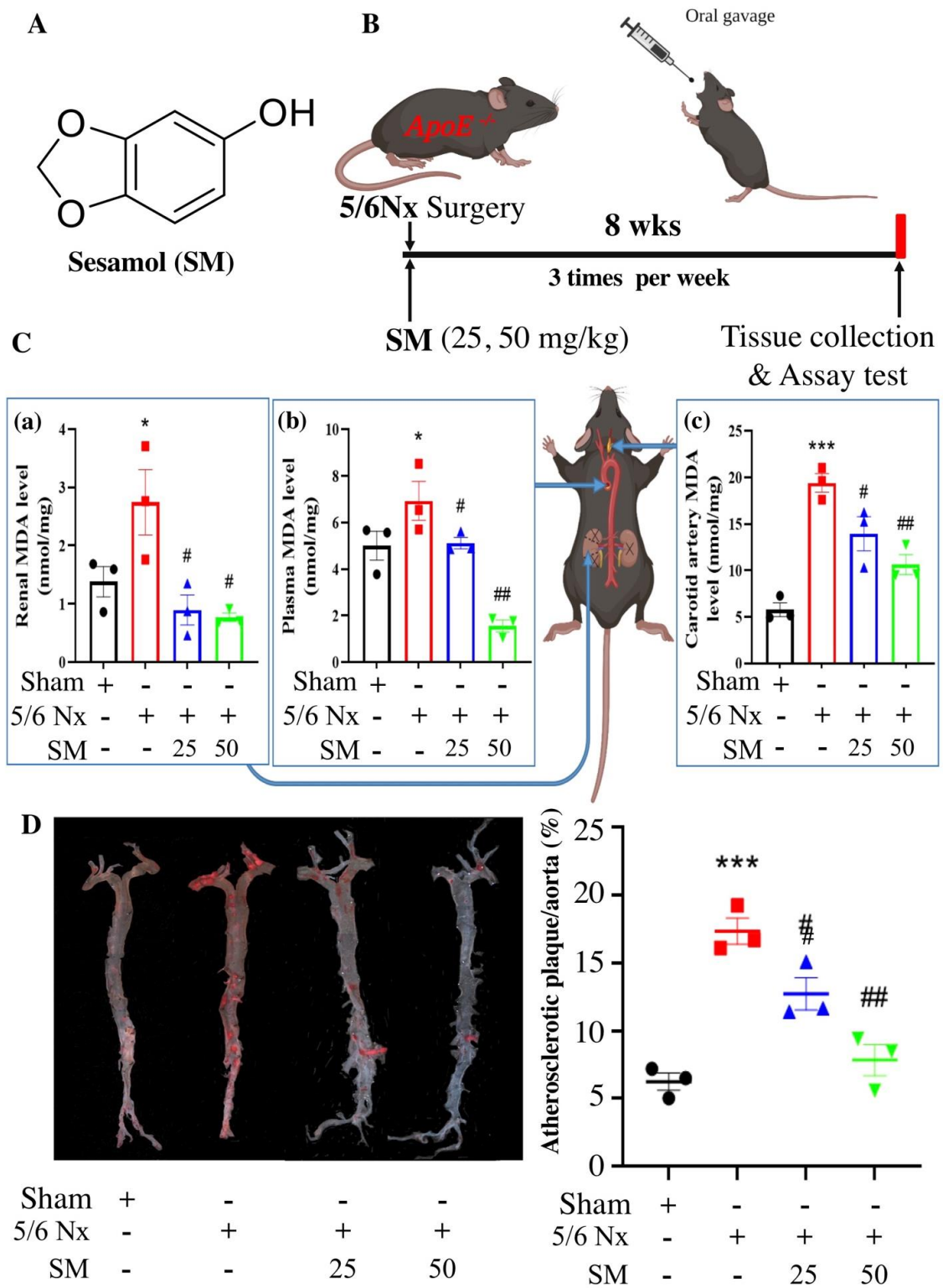


Figure 1. Sesamol (SM) reduces reactive oxygen species (ROS) levels and atherosclerosis in 5/6 Nx ApoE^{-/-} mice. **(A)** Structure of SM. **(B)** Schematic representation of the experimental mouse model. **(C)** Lipid peroxidation was assessed by measuring malondialdehyde (MDA) level. MDA level in (a) the kidney, (b) plasma, and (c) carotid artery in ApoE^{-/-} mice. **(D)** Representative aortas from mice in each group stained with Oil Red O and quantification of aortic root lesion sizes. Data are presented as mean ± SEM (*n* = 3 per group). * *p* < 0.05, *** *p* < 0.001 vs. sham group; # *p* < 0.05, ## *p* < 0.01 vs. 5/6 Nx group in ApoE^{-/-} mice.

2.3. Lipid Peroxidation Assay, Oil Red O Staining, and Histology Staining of Aortas

Experimental mice were anesthetized and euthanized via cervical dislocation, and the blood (to obtain plasma), carotid artery, aorta, and kidneys were collected. Lipid peroxidation was evaluated using a lipid peroxidation (MDA) assay kit (no. ab118970; Abcam, Cambridge, UK) according to the manufacturer's instructions. Atherosclerotic plaques were visualized using an Oil Red O Staining kit (Sigma), and images were captured with a Canon EOS 70D digital camera (Tokyo, Japan). The aortic roots and carotid artery were fixed overnight with 4% paraformaldehyde, after which 0.5% Oil Red O solution (Sigma-Aldrich) was used to stain the aortic roots for 24 h. The stained aorta were spread on the blackboard, and a digital camera was used to shoot under the same shooting parameters and the same lighting conditions. Carotid arteries were embedded in paraffin and serially sliced into 3 μm -thick sections. Every third slide from the serial sections was stained with hematoxylin and eosin (H&E), and images were captured using a Leica DM750 (Wetzlar, Germany). Images were analyzed using Image J (Version 1.52a, NIH, Bethesda, MD, USA).

2.4. Measurement of Cell Viability

For the cell viability assessment, 4×10^3 cells were seeded in 96-well plates. After incubation with SM (0.3–3 μM) or the control vehicle (0.1% DMSO) for 60 min, the cells were treated with or without H_2O_2 (100 μM) for 24 h. Thereafter, 20 μL of MTT solution (5 mg/mL) was added to each well, and the plate was incubated at 37 $^\circ\text{C}$ for 4 h. Next, the supernatant was replaced with DMSO. Then, the cells were oscillated. Finally, the absorbance of the sample at 570 nm was measured using a microplate reader (Infinite M1000, TECAN, Mechelen, Belgium). All data were normalized to those of the corresponding controls, and the percentage of control was calculated.

2.5. Measurement of Intracellular ROS Levels in Cells

Intracellular ROS levels were evaluated using a cellular ROS/superoxide detection assay kit (Abcam, Cambridge, UK) according to the manufacturer's instructions. Briefly, the cells were seeded at a density of 1.0×10^4 cells/well in 96-well plates, and they were allowed to attach for 24 h. Following this, the culture supernatant was removed, and cells were washed with phosphate-buffered saline (PBS). Next, the ROS-specific stain 2',7'-dichlorofluorescein diacetate (DCFH-DA) was added, and cells were incubated in the dark for 30 min at 37 $^\circ\text{C}$. Thereafter, the cells were washed twice with PBS. The cells were then observed via fluorescence microscopy, and intracellular ROS levels were measured using an Infinite M1000 microtiter plate reader (Tecan Group AG, Männedorf, Switzerland) (Ex = 488 nm, Em = 520 nm).

2.6. Apoptosis Assay

HAECs were incubated with SM (0.3–3 μM) or the control vehicle (0.1% DMSO) for 60 min, and they were then treated with or without H_2O_2 (100 μM) for 24 h. The treated cells were stained with 1 μM Hoechst 33,342 (Molecular Probes, Eugene, OR, USA) and calcein acetoxymethyl ester (calcein-AM) (Molecular Probes). Fluorescence imaging was performed with an Olympus IX70 inverted microscope (Tokyo, Japan), and apoptotic cells were quantified as previously described [11].

2.7. Protein Extraction and Western Blotting

Cells were seeded at a density of 2×10^5 cells/well into 6-well plates, and they were allowed to attach for 24 h. Subsequently, the cells were treated with vehicle, H_2O_2 (100 μM for 24 h) alone, or H_2O_2 (100 μM for 24 h) after SM pretreatment (0.3–3 μM for 1 h before the addition of H_2O_2). Subsequently, to obtain protein extracts, the cells were lysed and homogenized in RIPA lysis buffer in the presence of protease inhibitors (Roche Applied Science, Penzberg, Germany). The bovine serum albumin protein assay kit (Pierce Biotechnology Inc., Waltham, MA, USA) was used to measure protein con-

centrations. Cell lysates (containing 20 µg of protein) were loaded onto a 12% sodium dodecyl sulfate (SDS) polyacrylamide gel, and were separated by SDS polyacrylamide gel electrophoresis. The separated proteins were transferred onto a Hybond-PVDF membrane (GE Healthcare Amersham, Buckinghamshire), and were then blocked with SuperBlock (Pierce Biotechnology Inc.). Non-specific sites were blocked with blocking buffer (500 mL of 0.1% PBST containing 5 g PVP and 1.25 g BSA) for 1 h. For immunoblotting, the membranes were incubated overnight with one of the following primary antibodies at 4 °C: anti-p-IKK (1:1000; Cell Signaling, Danvers, MA, USA), anti-p53 (1:1000; Cell Signaling), anti-cleaved caspase-3 (1:1000; CC3, Cell Signaling), and anti-β-actin (1:10,000; Sigma) in PBST overnight at 4 °C. Anti-rabbit horseradish peroxidase-conjugated immunoglobulin G (1:1000; DakoCytomation, Glostrup, Denmark) in PBST (1 h, 37 °C) was used as a secondary antibody. β-Actin was used to verify an equal loading of proteins in each lane. Protein expression was assessed using ECL reagents (Millipore, Billerica, MA, USA), and was quantified using quantity video densitometry (G-box Image System; Syngene, Frederick, MD, USA) [11].

2.8. Quantitative Real-Time PCR

After homogenization of mice carotid arteries, samples were frozen with NucleoZOL at −80 °C, and the total RNA was isolated and extracted according to the manufacturer's instructions. The iScript cDNA Synthesis Kit (BioRad, Hercules, CA, USA) was used to synthesize cDNA. Finally, Q SYBR Green Supermix (BioRad) was used for real-time PCR. The primers are listed in Table 1.

Table 1. List of primers used in qPCR.

Gene Expression qPCR Primers		
<i>GAPDH</i>	5'-AGAAGGCTGGGGCTCATTG-3'	5'-AGGGGCCATCCACAGTCTTC-3'
<i>p53</i>	5'-TACAAGAAGTCACAGCACAT-3'	5'-GATAGTTCGGCGGTTTCAT-3'
<i>IKKα</i>	5'-GCCAGGGAGACTTGATGG-3'	5'-GAGGTCTGTGCTTTAGCTGCTT-3'
<i>Caspase-3</i>	5'-GCGATGGAGAATGTGCATAAATTC-3'	5'-GGGAAACCAACAGTACTCAGTCCT-3'

2.9. Statistical Analysis

Data are presented as mean ± standard error of mean (SEM) of *n* experiments. Data were compared using one-way analysis of variance (ANOVA) or *t*-test, where appropriate. Results with *p* < 0.05 were considered statistically significant. GraphPad Prism 5 software (GraphPad Software Inc., La Jolla, CA, USA) was used for all statistical analyses.

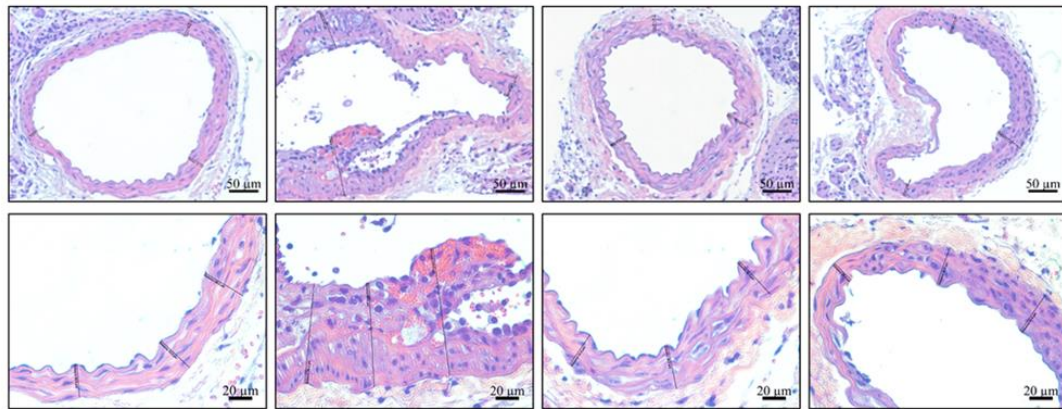
3. Results

3.1. Effects of SM on ROS Levels and Atherosclerosis in 5/6 Nx ApoE^{−/−} KO Mice

SM25- and SM50-treated 5/6 Nx ApoE^{−/−} mice showed no difference in body weight or mortality rate. To investigate the effect of SM on oxidative stress, we evaluated the effect of SM supplementation on lipid peroxidation by measuring the MDA level in the kidney, plasma, and carotid artery. Compared with the sham group, 5/6 Nx ApoE^{−/−} mice (5/6 Nx) group showed increased MDA levels. However, the MDA level in the SM25 and SM50 groups decreased compared with those in the 5/6 Nx group (Figure 1C (a–c)). Additionally, to investigate whether SM is an effective therapeutic agent for CKD-mediated atherosclerosis, we assessed the effect of SM on atherosclerotic lesions in 5/6 Nx ApoE^{−/−} mice. Compared with the sham mice, the 5/6 Nx mice showed significantly increased atherosclerotic lesions as assessed by Oil Red O staining of the aorta (2.83-fold increase) (5/6 Nx vs. sham; *p* < 0.001). The aortas from the SM25 and SM50 group mice showed significantly reduced staining patterns when compared with those from the 5/6 Nx mice, with reductions of 16.3% and 58.8%, respectively (Figure 1D). Furthermore, the mice administered SM demonstrated a significant attenuation of carotid artery plaque formation,

compared to the untreated mice. The plaque area was reduced after SM treatment in a dose-dependent manner (Figure 2A,B). At the 50 mg/kg dose, SM abrogated plaque formation, resulting in 70% reduction in plaque size compared to the untreated 5/6 Nx ApoE^{-/-} mice, as measured using morphometric analysis (Figure 2B, $p < 0.01$).

A



Sham	+	-	-	-
5/6 Nx	-	+	+	+
SM	-	-	25	50

B

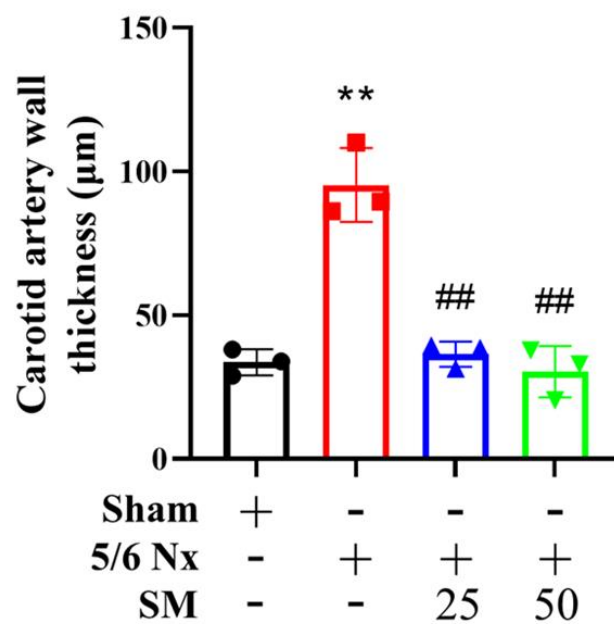


Figure 2. Hematoxylin and eosin staining shows the histopathology of atherosclerotic plaques. (A) Representative photomicrograph of ApoE^{-/-} mouse carotid artery (top panel, 200 \times and bottom panel, 400 \times). During the entire experiment, no obvious atherosclerotic lesions were found in the carotid artery of the sham group, and severe atherosclerosis was found in the carotid artery of the 5/6 Nx group. As the concentration of SM increased, the development of atherosclerotic lesions gradually decreased. (B) Wall thicknesses were quantified by unwitting researchers. Data are presented as mean \pm SEM ($n = 3$ per group). ** $p < 0.01$ vs. sham group; ## $p < 0.01$ vs. 5/6 Nx group in ApoE^{-/-} mice.

3.2. In Vitro Activity of SM on HAECs Injured Via H₂O₂ Treatment

We analyzed the effects of SM on H₂O₂-induced endothelial cell injury using cultured HAECs, and explored the underlying mechanisms. SM (3 μM) did not show any significant cytotoxic effect on HAECs, as determined using the MTT assay. Therefore, all subsequent experiments were conducted at doses less than 3 μM SM. To determine the protective effect of SM on H₂O₂-induced HAEC damage, cell survival was assessed using the MTT assay. The cells were pre-incubated with SM for 1 h and then with H₂O₂ (100 μM) for 24 h. HAEC viability significantly reduced after H₂O₂ treatment compared with control ($p < 0.001$, $n = 4$); however, pre-treatment with SM (0.3–3 μM) prevented the cell damage induced by 100 μM H₂O₂ ($p < 0.01$; $n = 4$; Figure 3A,B). These results suggest that SM might protect HAECs from ROS-related cellular damage. To further examine the protective effect of SM on H₂O₂-induced intracellular oxidative stress in HAECs, we measured intracellular ROS levels in H₂O₂-treated HAECs using DCFH-DA, an ROS-specific dye. Samples with higher concentration of ROS presented stronger green fluorescence intensity. The fluorescent intensity in H₂O₂-stimulated cells treated with SM (0.3, 1, and 3 μM) was weaker than that in H₂O₂-stimulated cells without any treatment (Figure 3C). Moreover, as shown in Figure 3D, H₂O₂ significantly increased intracellular ROS generation in HAECs ($p < 0.001$ vs. control, $n = 3$), and SM (0.3, 1, and 3 μM) treatment suppressed H₂O₂-induced ROS generation concentration-dependently ($p < 0.001$ at 3 μM vs. H₂O₂ alone; $n = 3$). Interestingly, the suppressive effect of 3 μM SM against H₂O₂-induced ROS generation was comparable to that of *N*-acetyl-L-cysteine (3 mM), a potent antioxidant.

3.3. Effects of SM on the Apoptosis of HAECs Exposed to H₂O₂

To elucidate whether SM suppresses H₂O₂-induced apoptosis in HAECs, cells were pretreated with increasing concentrations of SM (0.3–3 μM) and then exposed to H₂O₂ (100 μM). After 24 h, the cells were stained with Hoechst 33,342 and calcein-AM to assess nuclear morphology and membrane integrity. HAECs with condensed, fragmented nuclei were considered to be apoptotic. Fluorescence microscopy revealed that H₂O₂ alone induced cell apoptosis ($p < 0.001$), and pretreatment with SM suppressed H₂O₂-induced cell apoptosis dose dependently (0.3 μM, $p < 0.05$; 1 and 3 μM, $p < 0.01$ vs. H₂O₂-treated cells; Figure 4A,B).

3.4. Protective Effects of SM against H₂O₂-Induced Endothelial Cell Apoptosis Is Mediated via the IKKα Pathway

The levels of P-IKKα (a pro-inflammatory factor) and p53 (a pro-apoptotic factor) in H₂O₂-treated HAECs were determined by western blotting. As shown in Figure 5A, H₂O₂ treatment significantly increased the P-IKKα and p53 ($p < 0.001$ vs. control; $n = 4$) levels, whereas SM pretreatment significantly reduced the H₂O₂-mediated effects dose dependently (expression of P-IKKα, 0.3 μM and 1 μM SM, $p < 0.05$; 3 μM SM, $p < 0.01$ vs. H₂O₂ alone; $n = 4$; expression of p53, 0.3 and 1 μM SM, $p < 0.01$; 3 μM SM, $p < 0.001$ vs. H₂O₂ alone; $n = 4$). The effect of SM on cleaved caspase-3 (CC3) expression was also determined by Western blotting. The H₂O₂ treatment led to a significant increase in the CC3 level ($p < 0.001$, $n = 4$) in HAECs, and this effect was inhibited by 3 μM SM ($p < 0.001$, $n = 4$) (Figure 5A). We further evaluated whether the changes in p53 and CC3 expression were mediated by IKKα. We treated HAECs with si-IKKα and si-Ctl (control), and the expression levels of P-IKKα, p53, and CC3 were assessed by Western blotting. As shown in Figure 5B, the levels of P-IKKα, p53, and CC3 significantly increased in H₂O₂-treated HAECs ($p < 0.001$, $n = 4$); however, the levels of P-IKKα, p53, and CC3 decreased following pre-treatment of H₂O₂-treated HAECs with si-IKKα (P-IKKα and CC3, $p < 0.001$ and p53, $p < 0.05$ vs. H₂O₂-treated alone; $n = 4$, Figure 5B). Additionally, in vivo quantitative real-time PCR analysis showed that the mRNA level of *IKKα*, *p53*, and *caspase 3* or Western blotting data showed protein levels of P-IKKα, p53, and CC3 were significantly increased in the carotid artery of 5/6 Nx ApoE^{-/-} mice compared with sham group (Figure 5C–F), whereas they were decreased in the carotid artery of 5/6 Nx

ApoE^{-/-} mice pretreated with SM (Figure 5C–F). These results indicated that H₂O₂ induced apoptosis via the P-IKKα/p53/CC3 pathway.

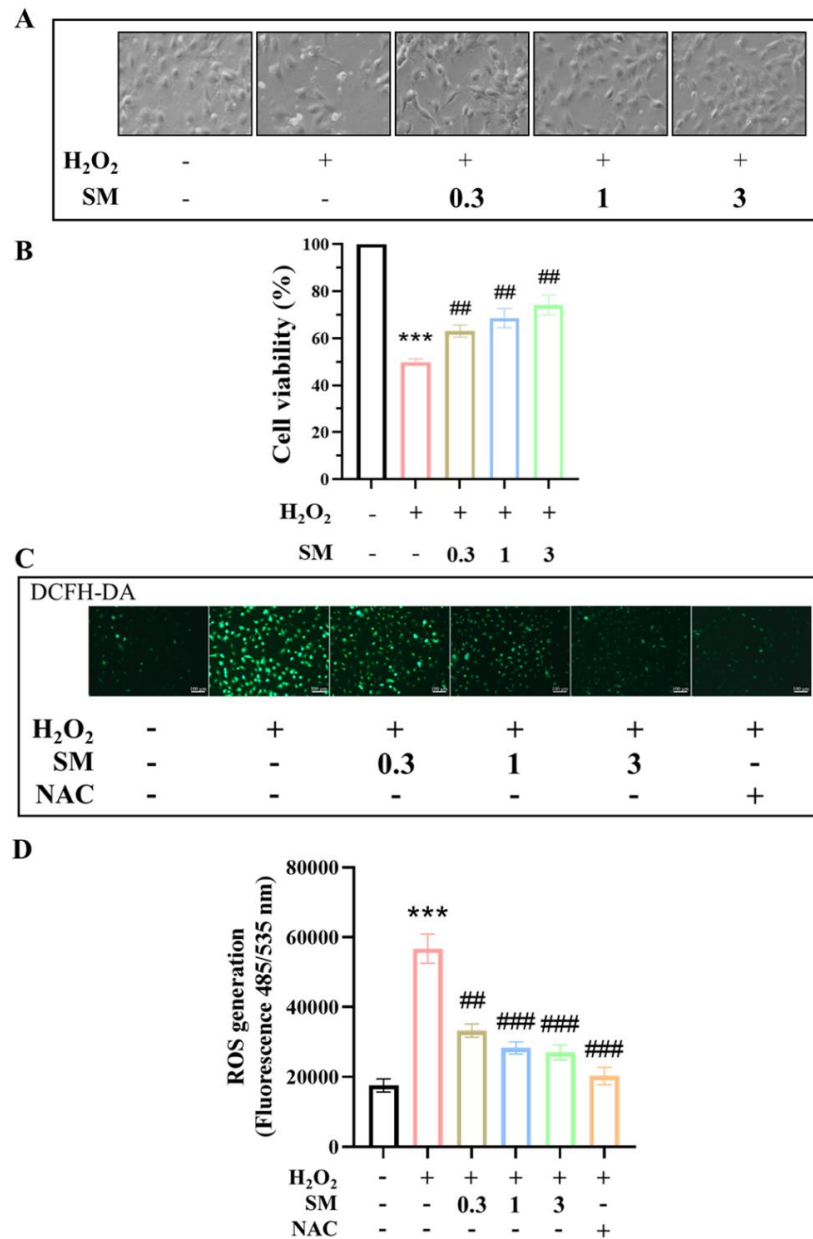


Figure 3. Effect of SM on the viability and intracellular ROS production of H₂O₂-treated human aortic endothelial cells (HAECs). (A) Representative images showing the effect of SM (0.3–3 μM) on HAEC morphological injury induced by H₂O₂ observed under a light microscope. (B) Following pretreatment with different concentrations of SM (0.3–3 μM) for 1 h, HAECs were treated with H₂O₂ (100 μM) for another 24 h; cell viability increased in a dose-dependent manner following SM treatment. Cell viability was determined using MTT assay. (C) A typical fluorescence image captured using a fluorescence microscope using 2',7'-dichlorofluorescein diacetate to stain HAECs after H₂O₂ stimulation and SM incubation to observe intracellular ROS intensity; scale bar = 100 μm. (D) Cellular ROS/superoxide detection assay was performed. Data are presented as mean ± SEM. *p* values were determined using Student's *t*-test. (***) *p* < 0.001 vs. control group, ** *p* < 0.01, *** *p* < 0.001 vs. H₂O₂ group). *N*-acetyl-L-cysteine (NAC, 3 mM).

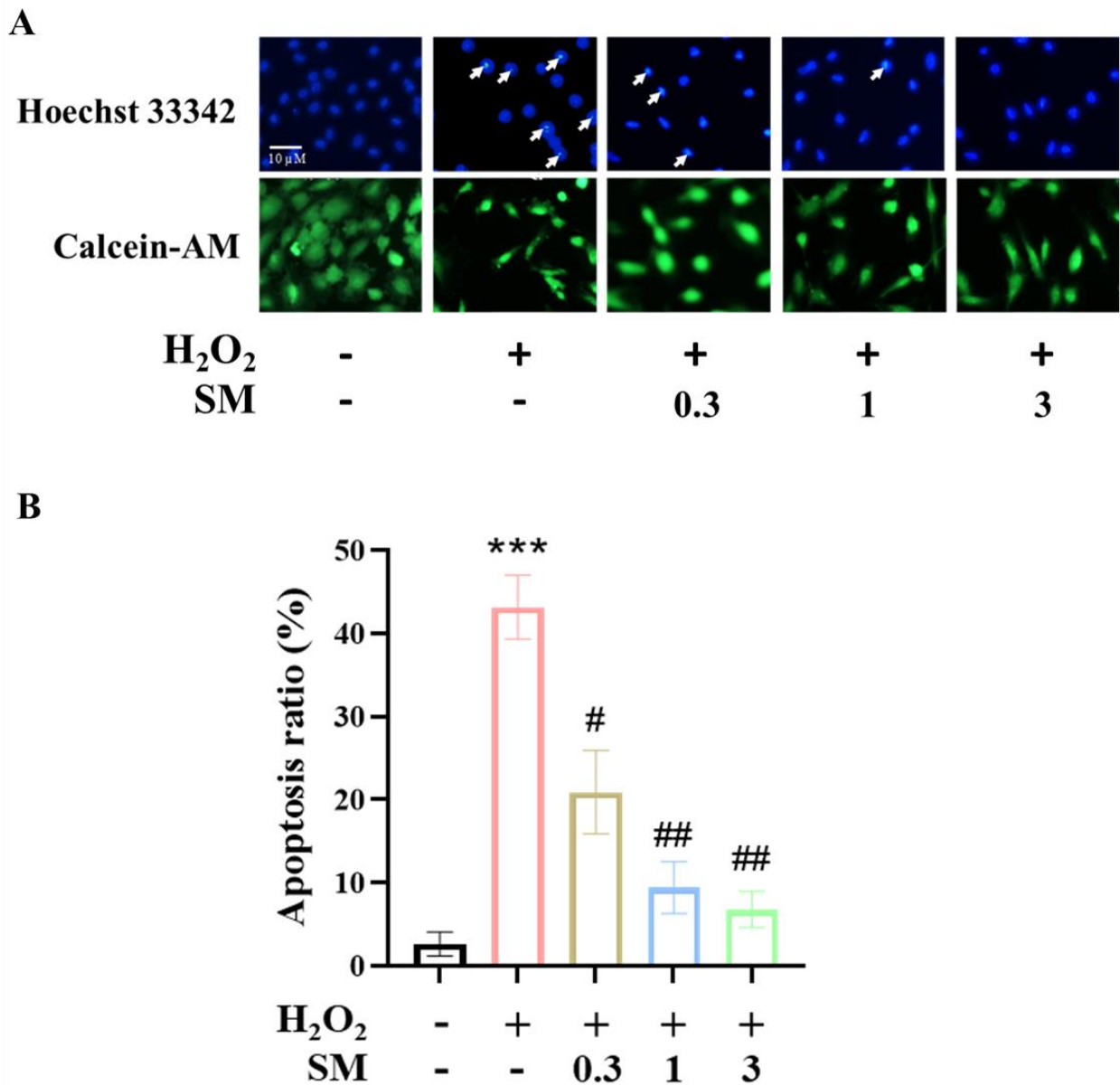


Figure 4. Protective effects of SM against H₂O₂-induced apoptosis in HAECs. HAECs were pretreated with SM (0.3–3 μM) for 30 min, and then incubated with or without 100 μM H₂O₂ for 24 h. (A) Epifluorescence microscopy images were obtained after staining with Hoechst 33,342 to assess nuclear morphology, and calcein-AM to evaluate membrane integrity. The presence of condensed and fragmented nuclei was considered an indicator of apoptosis (white arrow). (B) The mean percent cell apoptosis was evaluated in quadruplicate samples. The *p* values were determined using Student’s *t*-test. *** *p* < 0.001 vs. control group; # *p* < 0.05, ## *p* < 0.01 vs. H₂O₂-treated cells.

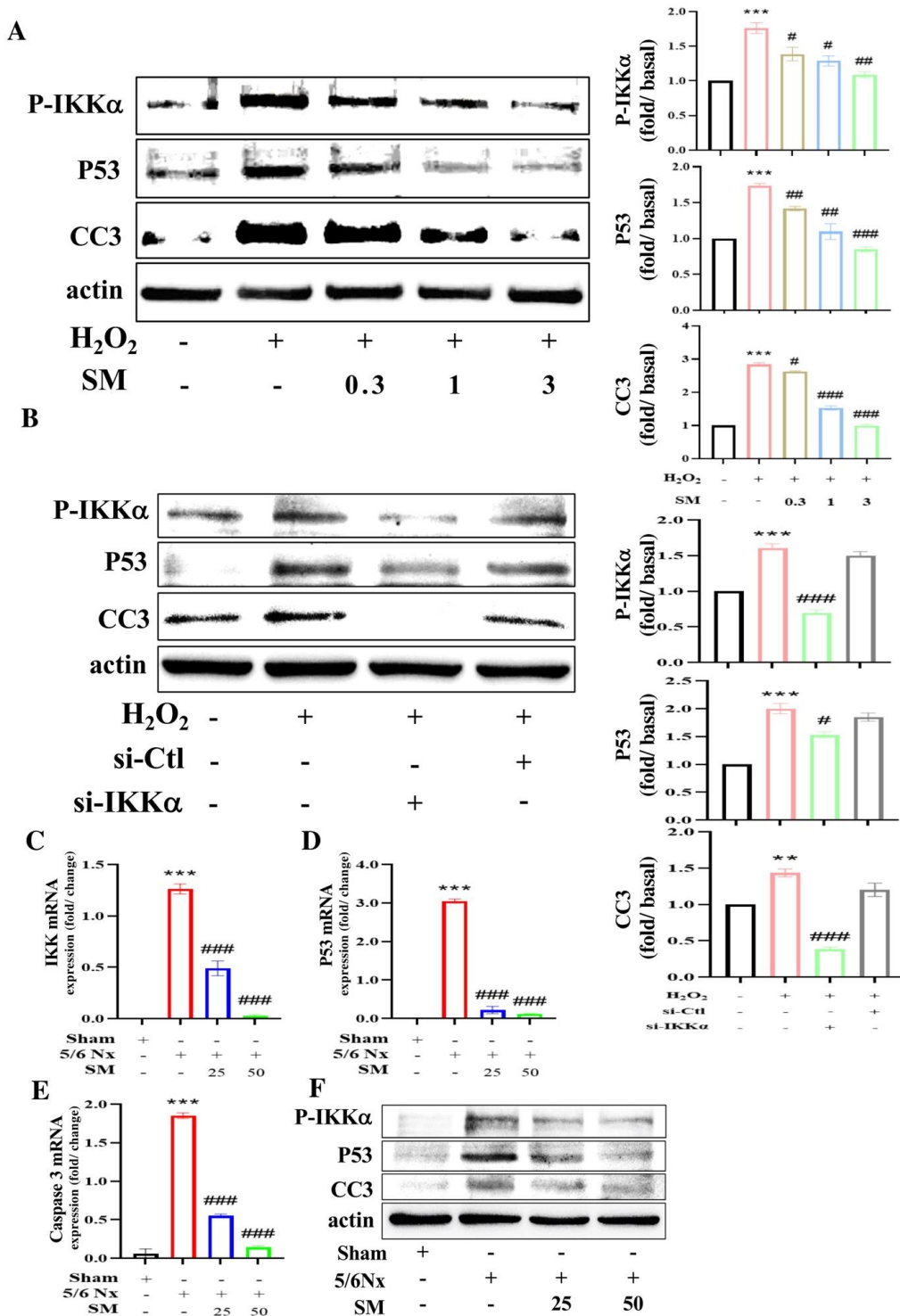


Figure 5. H₂O₂ significantly induces apoptosis in HAECs via the IKKα pathway, and pretreatment with SM blocks the activation of this pathway. (A) Western blot showing the effect of SM on the protein expression of P-IKKα, p53, and CC3 in H₂O₂-treated HAECs. (B) Western blotting showed that H₂O₂ induces apoptosis of HAECs via the IKKα pathway. In addition to H₂O₂, HAECs were treated with si-IKKα and si-Ctl (control). *p* values were determined using Student’s *t*-test. ** *p* < 0.01, *** *p* < 0.001 vs. control group; # *p* < 0.05, ## *p* < 0.01, and ### *p* < 0.001 vs. H₂O₂-treated cells. mRNA levels of (C) *IKKα*, (D) *p53*, and (E) *caspase-3* and (F) protein levels of P-IKKα, p53, and CC3 in the carotid arteries of SM-treated or untreated 5/6 Nx ApoE^{-/-} mice and sham were measured using quantitative real-time PCR, and they were normalized to the level of GAPDH mRNA. Data are presented as mean ± SEM (*n* = 3 per group). *** *p* < 0.001 vs. sham group; ### *p* < 0.001 vs. 5/6 Nx group in ApoE^{-/-} mice.

4. Discussion

In the present study, we demonstrated that 5/6 Nx ApoE^{-/-} mice showed significantly increased levels of MDA in the kidney, plasma, and carotid artery, indicating lipid peroxidation, and increased numbers of atherosclerotic lesions in the aorta and carotid artery, as assessed by Oil Red O staining and hematoxylin and eosin staining, respectively. Furthermore, these effects were significantly attenuated by SM treatment. SM could also suppress H₂O₂-induced oxidative stress and injury in HAECs. Moreover, the data suggested that this may be mediated by a reduction in the level of P-IKK α and an inhibition of the p53/caspase-3 pathway in HAECs. These findings indicate that SM improved ROS-induced endothelial cell damage and atherosclerotic CVD due to renal injury. Thus, renal injury potentiated atherosclerosis, which is consistent with clinical observations and past experimental evidence [22].

The increased risk of premature death in patients with chronic renal failure is associated with the systemic, chronic pro-inflammatory state in CKD, which contributes to a remodeling of the blood vessels and the myocardium, leading to the formation of atherosclerotic lesions [1]. A suggested link between CKD and CVD is endothelial dysfunction and oxidative stress [22]. The consequences of oxidative stress in patients with CKD include atherosclerosis, protein denaturation, and a shortened red blood cell life span. An increase in ROS levels possibly triggers the remodeling of blood vessels and myocardium, leading to the formation of atherosclerotic lesions [3]. Therefore, studying the mechanism of ROS generation in CKD-mediated atherosclerosis and the potential interventions to protect endothelial cells from ROS-induced injury can be beneficial to prevent CVD [2,23].

SM has a vital role in diminishing endothelial oxidative stress [24]. SM reduces ROS generation in human neuronal cells exposed to H₂O₂ [13]. In the present study, SM inhibited ROS production induced by H₂O₂ in HAECs. These results indicate that SM exerted a protective effect by inhibiting H₂O₂-induced cell injury. High concentrations of SM are cytotoxic to hepatocellular carcinoma cells [12]. Our findings showed that SM has a protective effect at all tested concentrations (0.3, 1, and 3 μ M), and that it had no effect on the viability of HAECs, which suggested that SM exerted beneficial effects on the endothelium without any negative adverse effects. ROS are produced during normal cellular metabolism [25]. When there is an imbalance between the levels of free radicals generated and antioxidant defense systems, excessive ROS is generated, which can damage proteins and DNA, leading to endothelial dysfunction [23]. This contributes to the progression of cerebral and vascular diseases [2,4,8]. H₂O₂ plays a considerable role in vascular and endothelial dysfunction [23]. High levels of H₂O₂ can induce significant injury and diminish endothelial cell viability [6,23]. Our results also showed that H₂O₂ significantly reduced cell viability and resulted in DNA damage in HAECs. However, pre-incubation of the cells with SM 1 h before the addition of H₂O₂ significantly suppressed H₂O₂-induced cell death. These results demonstrate the anti-apoptotic property of SM.

The ternary IKK complex comprises IKK α , IKK β , and IKK γ (NEMO) [26], and signaling through this complex induces the activation of nuclear factor kappa-B (NF- κ B), involved in cancer, immune responses, inflammation, and cell survival [26,27]. IKK α is stimulated by H₂O₂ [28]. Additionally, IKK α plays a key role in p53-induced cell apoptosis [29]. To elucidate the mechanisms involved in the protection of endothelial cells by SM against oxidative stress injury, we investigated the effects of SM on IKK α and p53 activation in HAECs exposed to H₂O₂. IKK α mediated the stimulation of p53 activation in HAECs treated with H₂O₂. These results suggest that IKK α plays a supportive role in ROS-mediated apoptosis by modulating p53 transcriptional activity.

Caspase-3 is an effective indicator of the degree of cellular apoptosis [30]. Caspase-3 is mainly activated via chromatin condensation and DNA fragmentation in the nucleus [30]. Caspase-3 is the main protease involved in the apoptosis of endothelial cells as it functions downstream of other caspases and is involved in initiating the apoptotic cascade [11,30]. In this study, caspase-3 activation was increased by H₂O₂ in HAECs, and this could be prevented by pretreating cells with an siRNA targeting IKK α . Furthermore, the *in vivo*

mRNA expression of IKK α , p53, and caspase-3, or the protein expression of P-IKK α , p53, and cleaved caspase-3 decreased in the carotid artery tissues of 5/6 Nx ApoE^{-/-} mice following SM treatment, similar to those observed in in vitro experiments. Based on these findings, we hypothesize that H₂O₂-induced apoptosis and atherosclerosis occurs via the IKK α /p53/caspase-3 pathway and that SM can inhibit the activity of this pathway.

As mentioned earlier, the ROS generated in CKD can oxidize biomolecules such as lipids, which further increases cell toxicity, kidney injury, and atherosclerosis [4,31]. Additionally, sesamol, a major constituent of sesame oil, reportedly inhibits lipid peroxidation in rat livers and kidneys [32]. Our results showed that in 5/6 Nx ApoE^{-/-} mice, SM protected the endothelial cells and arrested atherosclerosis to attenuate ROS-injury arising as a result of chronic kidney injury. SM administration reportedly improves ferric-nitrosyltriacetate-induced acute kidney injury in mice, which supports our findings [17]. In addition, kidney damage caused by other factors, including glomerular lipidosis—associated with dyslipidemic conditions prone to the development of kidney disease—or a dramatic increase in immune/inflammatory responses can worsen atherosclerosis and impact the occurrence of atherosclerotic artery disease [33,34]. In our preliminary data, kidney hematoxylin and eosin staining revealed that the 5/6 Nx group had increased glomerular lipidosis, which can lead to decreased kidney function [33]. Meanwhile, glomerular lipidosis was decreased in the 5/6 Nx mice treated with SM; within this group, SM was found to protect against ROS injury and ameliorate ROS-induced glomeruli damage. Moreover, in our preliminary data, in addition to improving the direct endothelium impact in the nephropathy 5/6 mouse model, SM has beneficial effects on kidney function while improving traditional risk factors related to arteriosclerosis. In addition, SM appeared to improve the inflammation caused in the 5/6 nephropathy model. Hence, SM may represent a promising treatment for kidney disease.

ROS from other sources, including advanced glycation end products (AGEs) or mitochondrial-derived ROS can also contribute to endothelial cell damage and CVD [6,8,23,35,36]. In the present study, we exclusively focused on ROS generation in response to exogenous H₂O₂; hence, further investigation into AGEs and mitochondrial ROS are needed to elucidate their role in cell damage. Additionally, although antioxidant strategies have potential, only a few interventional studies have examined their effects. Hence, large, randomized, long-term studies are required to establish the efficacy and safety of SM in patients with CKD.

5. Conclusions

Overall, SM could inhibit H₂O₂-induced endothelial cell injury by direct inhibition of intracellular ROS generation. These protective effects were closely associated with the suppression of IKK α phosphorylation and inhibition of the apoptotic death cascade through the suppression of p53 and a reduction in caspase-3 activation. Additionally, SM also improved CKD-related outcomes in the 5/6 Nx mouse model of CKD-induced atherosclerosis. The findings provide an important basis to better understand the action of SM on HAECs and the potential beneficial effects of SM treatment in CKD and CVD.

Author Contributions: Conceptualization, J.-S.W., P.-H.T. and M.-Y.S.; methodology, P.-H.T., K.-F.T. and F.-Y.C.; software, J.-S.W.; validation, J.-S.W., P.-H.T. and M.-Y.S.; formal analysis, M.-Y.S.; investigation, P.-H.T.; resources, M.-Y.S.; data curation, P.-H.T.; writing—original draft preparation, J.-S.W. and M.-Y.S.; writing—review and editing, M.-Y.S.; visualization, M.-Y.S.; supervision, W.-C.Y. and M.-Y.S.; project administration, M.-Y.S. and F.-Y.C.; funding acquisition, M.-Y.S. All authors have read and agreed to the published version of the manuscript.

Funding: This research was funded by the Ministry of Science and Technology of Taiwan (MOST108-2320-B-039-034-MY3), China Medical University (CMU109-MF-70 and CMU110-MF-41), and China Medical University Hospital (DMR-106-118, DMR-108-127, DMR-109-142 and DMR-110-144).

Institutional Review Board Statement: The study was performed in accordance with the Guide for the Care and Use of Laboratory Animals, published by the U.S. National Institutes of Health, and it was approved by the China Medical University Institutional Animal Care and Use Committee (permit no. CMUIACUC-2019-094).

Informed Consent Statement: Not applicable.

Data Availability Statement: The data presented in this study are available in article.

Acknowledgments: The diagram was created using BioRender (<https://biorender.com/>, accessed on 9–24 July 2021).

Conflicts of Interest: The authors declare no conflict of interest.

References

1. Wanner, C.; Amann, K.; Shoji, T. The heart and vascular system in dialysis. *Lancet* **2016**, *388*, 276–284. [[CrossRef](#)]
2. Pizzino, G.; Irrera, N.; Cucinotta, M.; Pallio, G.; Mannino, F.; Arcoraci, V.; Squadrito, F.; Altavilla, D.; Bitto, A. Oxidative Stress: Harms and Benefits for Human Health. *Oxid. Med. Cell. Longev.* **2017**, *2017*, 8416763. [[CrossRef](#)]
3. Rapa, S.F.; Di Iorio, B.R.; Campiglia, P.; Heidland, A.; Marzocco, S. Inflammation and Oxidative Stress in Chronic Kidney Disease—Potential Therapeutic Role of Minerals, Vitamins and Plant-Derived Metabolites. *Int. J. Mol. Sci.* **2019**, *21*, 263. [[CrossRef](#)] [[PubMed](#)]
4. Granger, D.N.; Kvietys, P.R. Reperfusion injury and reactive oxygen species: The evolution of a concept. *Redox Biol.* **2015**, *6*, 524–551. [[CrossRef](#)] [[PubMed](#)]
5. Wu, Y.; Wang, Y.; Nabi, X. Protective effect of Ziziphora clinopodioides flavonoids against H₂O₂-induced oxidative stress in HUVEC cells. *Biomed. Pharm.* **2019**, *117*, 109156. [[CrossRef](#)] [[PubMed](#)]
6. Park, W.H. The effects of exogenous H₂O₂ on cell death, reactive oxygen species and glutathione levels in calf pulmonary artery and human umbilical vein endothelial cells. *Int. J. Mol. Med.* **2013**, *31*, 471–476. [[CrossRef](#)]
7. Sorriento, D.; Santulli, G.; Del Giudice, C.; Anastasio, A.; Trimarco, B.; Iaccarino, G. Endothelial cells are able to synthesize and release catecholamines both in vitro and in vivo. *Hypertension* **2012**, *60*, 129–136. [[CrossRef](#)] [[PubMed](#)]
8. Panth, N.; Paudel, K.R.; Parajuli, K. Reactive Oxygen Species: A Key Hallmark of Cardiovascular Disease. *Adv. Med. Sci.* **2016**, *2016*, 9152732. [[CrossRef](#)]
9. Liu, C.; Huang, Y. Chinese Herbal Medicine on Cardiovascular Diseases and the Mechanisms of Action. *Front. Pharm.* **2016**, *7*, 469. [[CrossRef](#)]
10. Mashour, N.H.; Lin, G.I.; Frishman, W.H. Herbal medicine for the treatment of cardiovascular disease: Clinical considerations. *Arch. Intern Med.* **1998**, *158*, 2225–2234. [[CrossRef](#)]
11. Chen, W.Y.; Chen, F.Y.; Lee, A.S.; Ting, K.H.; Chang, C.M.; Hsu, J.F.; Lee, W.S.; Sheu, J.R.; Chen, C.H.; Shen, M.Y. Sesamol reduces the atherogenicity of electronegative L5 LDL in vivo and in vitro. *J. Nat. Prod.* **2015**, *78*, 225–233. [[CrossRef](#)]
12. Liu, Z.; Ren, B.; Wang, Y.; Zou, C.; Qiao, Q.; Diao, Z.; Mi, Y.; Zhu, D.; Liu, X. Sesamol Induces Human Hepatocellular Carcinoma Cells Apoptosis by Impairing Mitochondrial Function and Suppressing Autophagy. *Sci. Rep.* **2017**, *7*, 45728. [[CrossRef](#)]
13. Ruankham, W.; Suwanjang, W.; Wongchitrat, P.; Prachayasittikul, V.; Prachayasittikul, S.; Phopin, K. Sesamin and sesamol attenuate H₂O₂-induced oxidative stress on human neuronal cells via the SIRT1-SIRT3-FOXO3a signaling pathway. *Nutr. Neurosci.* **2019**, *24*, 90–101. [[CrossRef](#)]
14. Henrich, T.J.; Hatano, H.; Bacon, O.; Hogan, L.E.; Rutishauser, R.; Hill, A.; Kearney, M.F.; Anderson, E.M.; Buchbinder, S.P.; Cohen, S.E.; et al. HIV-1 persistence following extremely early initiation of antiretroviral therapy (ART) during acute HIV-1 infection: An observational study. *PLoS Med.* **2017**, *14*, e1002417. [[CrossRef](#)]
15. Sharma, S.; Kaur, I.P. Development and evaluation of sesamol as an antiaging agent. *Int. J. Derm.* **2006**, *45*, 200–208. [[CrossRef](#)] [[PubMed](#)]
16. Singh, N.; Khullar, N.; Kakkar, V.; Kaur, I.P. Hepatoprotective effects of sesamol loaded solid lipid nanoparticles in carbon tetrachloride induced sub-chronic hepatotoxicity in rats. *Environ. Toxicol.* **2016**, *31*, 520–532. [[CrossRef](#)] [[PubMed](#)]
17. Hsu, D.Z.; Wan, C.H.; Hsu, H.F.; Lin, Y.M.; Liu, M.Y. The prophylactic protective effect of sesamol against ferric-nitrosyltriacetate-induced acute renal injury in mice. *Food Chem. Toxicol.* **2008**, *46*, 2736–2741. [[CrossRef](#)] [[PubMed](#)]
18. Xie, W.; Zhou, P.; Sun, Y.; Meng, X.; Dai, Z.; Sun, G.; Sun, X. Protective Effects and Target Network Analysis of Ginsenoside Rg1 in Cerebral Ischemia and Reperfusion Injury: A Comprehensive Overview of Experimental Studies. *Cells* **2018**, *7*, 270. [[CrossRef](#)] [[PubMed](#)]
19. Kim, J.W.; Byun, M.S.; Yi, D.; Lee, J.H.; Jeon, S.Y.; Jung, G.; Lee, H.N.; Sohn, B.K.; Lee, J.Y.; Kim, Y.K.; et al. Coffee intake and decreased amyloid pathology in human brain. *Transl. Psychiatry* **2019**, *9*, 270. [[CrossRef](#)]
20. Zhang, B.; Saatman, K.E.; Chen, L. Therapeutic potential of natural compounds from Chinese medicine in acute and subacute phases of ischemic stroke. *Neural Regen. Res.* **2020**, *15*, 416–424.
21. Wiese, C.B.; Zhong, J.; Xu, Z.Q.; Zhang, Y.; Ramirez Solano, M.A.; Zhu, W.; Linton, M.F.; Sheng, Q.; Kon, V.; Vickers, K.C. Dual inhibition of endothelial miR-92a-3p and miR-489-3p reduces renal injury-associated atherosclerosis. *Atherosclerosis* **2019**, *282*, 121–131. [[CrossRef](#)]

22. Cachofeiro, V.; Goicochea, M.; de Vinuesa, S.G.; Oubina, P.; Lahera, V.; Luno, J. Oxidative stress and inflammation, a link between chronic kidney disease and cardiovascular disease. *Kidney Int. Suppl.* **2008**, *74*, S4–S9. [[CrossRef](#)] [[PubMed](#)]
23. Cai, H.; Harrison, D.G. Endothelial dysfunction in cardiovascular diseases: The role of oxidant stress. *Circ. Res.* **2000**, *87*, 840–844. [[CrossRef](#)] [[PubMed](#)]
24. Geetha, T.; Rohit, B.; Pal, K.I. Sesamol: An efficient antioxidant with potential therapeutic benefits. *Med. Chem.* **2009**, *5*, 367–371. [[CrossRef](#)] [[PubMed](#)]
25. Snezhkina, A.V.; Kudryavtseva, A.V.; Kardymon, O.L.; Savvateeva, M.V.; Melnikova, N.V.; Krasnov, G.S.; Dmitriev, A.A. ROS Generation and Antioxidant Defense Systems in Normal and Malignant Cells. *Oxid. Med. Cell Longev.* **2019**, *2019*, 6175804. [[CrossRef](#)]
26. Hacker, H.; Karin, M. Regulation and function of IKK and IKK-related kinases. *Sci. STKE* **2006**, *2006*, re13. [[CrossRef](#)]
27. Hayden, M.S.; Ghosh, S. Shared principles in NF-kappaB signaling. *Cell* **2008**, *132*, 344–362. [[CrossRef](#)]
28. Kamata, H.; Manabe, T.; Oka, S.; Kamata, K.; Hirata, H. Hydrogen peroxide activates IkappaB kinases through phosphorylation of serine residues in the activation loops. *FEBS Lett.* **2002**, *519*, 231–237. [[CrossRef](#)]
29. Huang, W.C.; Ju, T.K.; Hung, M.C.; Chen, C.C. Phosphorylation of CBP by IKKalpha promotes cell growth by switching the binding preference of CBP from p53 to NF-kappaB. *Mol. Cell* **2007**, *26*, 75–87. [[CrossRef](#)]
30. Thornberry, N.A.; Lazebnik, Y. Caspases: Enemies within. *Science* **1998**, *281*, 1312–1316. [[CrossRef](#)]
31. Shen, M.Y.; Chen, F.Y.; Hsu, J.F.; Fu, R.H.; Chang, C.M.; Chang, C.T.; Liu, C.H.; Wu, J.R.; Lee, A.S.; Chan, H.C.; et al. Plasma L5 levels are elevated in ischemic stroke patients and enhance platelet aggregation. *Blood* **2016**, *127*, 1336–1345. [[CrossRef](#)]
32. Kang, M.H.; Naito, M.; Tsujihara, N.; Osawa, T. Sesamol inhibits lipid peroxidation in rat liver and kidney. *J. Nutr.* **1998**, *128*, 1018–1022. [[CrossRef](#)]
33. Manzini, S.; Busnelli, M.; Parolini, C.; Minoli, L.; Ossoli, A.; Brambilla, E.; Simonelli, S.; Lekka, E.; Persidis, A.; Scanziani, E.; et al. Topiramate protects apoE-deficient mice from kidney damage without affecting plasma lipids. *Pharm. Res.* **2019**, *141*, 189–200. [[CrossRef](#)] [[PubMed](#)]
34. Busnelli, M.; Manzini, S.; Bonacina, F.; Soldati, S.; Barbieri, S.S.; Amadio, P.; Sandrini, L.; Arnaboldi, F.; Donetti, E.; Laaksonen, R.; et al. Fenretinide treatment accelerates atherosclerosis development in apoE-deficient mice in spite of beneficial metabolic effects. *Br. J. Pharm.* **2020**, *177*, 328–345. [[CrossRef](#)] [[PubMed](#)]
35. Yin, M.C. Inhibitory effects and actions of pentacyclic triterpenes upon glycation. *BioMedicine* **2015**, *5*, 13. [[CrossRef](#)] [[PubMed](#)]
36. Liu, Z.; Lv, Y.; Zhang, Y.; Liu, F.; Zhu, L.; Pan, S.; Qiu, C.; Guo, Y.; Yang, T.; Wang, J. Matrine-Type Alkaloids Inhibit Advanced Glycation End Products Induced Reactive Oxygen Species-Mediated Apoptosis of Aortic Endothelial Cells In Vivo and In Vitro by Targeting MKK3 and p38MAPK Signaling. *J. Am. Heart Assoc.* **2017**, *6*, e007441. [[CrossRef](#)] [[PubMed](#)]